Robust shape-retaining nanocellulose-based aerogels decorated with silver nanoparticles for fast continuous catalytic discoloration of organic dyes

Zhang, Weihua; Wang, Xiaoju; Zhang, Yongchao; van Bochove, Bas; Mäkilä, Ermei; Seppälä, Jukka; Xu, Chunlin; Willför, Stefan; Xu, Wen Yang

Published in:
Separation and Purification Technology

DOI:
10.1016/j.seppur.2020.116523

Published: 24/03/2020

Document Version
Accepted author manuscript

Document License
CC BY-NC-ND

Robust shape-retaining nanocellulose-based aerogels decorated with silver nanoparticles for fast continuous catalytic discoloration of organic dyes

Weihua Zhang [a], Xiaoju Wang [a], Yongchao Zhang [a], Bas van Bochove [b], Jukka Seppälä [b], Wenyang Xu [a], Stefan Willför [a], Chunlin Xu [a*]

[a] Research Group of Wood and Paper Chemistry, Laboratory of Natural Materials Technology, Åbo Akademi University, Turku FI-20500, Finland

[b] Polymer Technology, Department of Chemical and Metallurgical Engineering, Aalto University, Kemistintie 1, 02150 Espoo, Finland

Corresponding authors

* Johan Gadolin Process Chemistry Centre, c/o Laboratory of Wood and Paper Chemistry, Åbo Akademi University, Turku FI-20500, Finland. E-mail: cxu@abo.fi; Tel: +358 40 8362088

Abstract:

In this work we present a green method to prepare aerogel membranes based on cellulose nanofibers (CNFs) crossed-linked with poly (ethylene imine) (PEI) and further decorated with silver nanoparticles (Ag NPs). The nanosized Ag NPs were reduced and immobilized on the surface of the pore walls inside the aerogel. The as-prepared composite aerogel membrane showed excellent continuous catalytic discoloration of aqueous cationic and anionic dye solutions in batch and flow filtration tests. Moreover, the aerogel membrane exhibited very stable catalytic activity with discoloration efficiency at as high as 98% after 10 times reuse and the water permeance was high, up to 5×10^4 $L.m^{-2}$ h^{-1}. Interestingly, the aerogel membrane showed excellent shape recovery in water and no obvious deterioration of the structure was observed during long time testing. Therefore, the obtained aerogel membranes showed great potential in waste water treatment and catalytic applications.

Keywords: Nanocellulose aerogels, Wet strength, Silver nanoparticles, dye discoloration

1. Introduction

Nowadays, the rapid industrialization and urbanization, population growth, and climate change have caused serious water pollution worldwide and decreased the quality of human life [1-4]. Industrial wastewater that contains organic pollutants, heavy metals, and dyes is one of the most critical water polluting sources. Especially organic dyes, such as methylene blue (MB), Congo red (CR), methylene orange (MO), or rhodamine 6G (Rh6G) are threating water cleaning as they are highly toxic, chemically stable, and difficult to degrade. Moreover, these dyes are still used widely in the printing and textile industries for producing paints, cloth, leather, and paper and thus generate dye waste streams [5, 6]. These dye-polluted streams are threatening the quality of water on this planet, influencing the ecological balance, and will eventually cause severe harm to all human beings [7-11]. In order to treat dye-contaminated water efficiently, vast technologies, such as physical adsorption [12, 13], membrane filtration [14, 15], photo-catalytic degradation [16, 17], oxidation [18, 19],

catalytic reduction [20-22], and biodegradation [23, 24], have been developed and used in recent years. However, there are some limits about these traditional methods. For example, the efficiency of adsorption and membrane filtration methods is usually low, and they also produce solid wastes [15, 25]. In addition, the regeneration process for adsorbents and membranes is time-, money-, and energy-consuming. Photo-catalysts such as CdS [26], ZnO [27], TiO_2 [28], and their composites have been developed and widely applied in organic dye degradation. However, the photo-catalytic process usually needs intensive light to irradiate the photo-catalysts to generate strong oxidation intermediates, which means this process would consume a large amount of energy. Biodegradation is difficult to be used in industrial-scale applications because of its high cost and low efficiency. Recently, catalytic reduction of organic dyes caused attention for its high efficiency and being easy to process. Noble metal particles are usually used as catalysts for catalyzing organic dye reduction processes. Ag NPs as an important noble metal catalyst plays an important role in catalyzing discoloration of organic dyes for its excellent catalytic performance [29]. However, Ag NPs easily aggregate in solution because their high surface energy results in the diminishment of their catalytic efficiency [22, 30].

In recent years, nanocellulose (CNC, CNF, and bacterial cellulose) and its derivatives have been studied widely and showed great potential in applications such as cosmetics, food, energy, water treatment, and medical industries due to their high surface area, being environmental friendly, abundance in nature, thermal stability, functional surface, and easy processing [31-34]. Among these applications nanocellulose as a support for metal nanoparticles to prevent the aggregation problem has attracted a wide interest [31]. Nanocellulose can dramatically improve the stability and dispersibility of the metal nanoparticles in solutions and increase the catalytic efficiency [35]. However, the recovery of the catalyst from solution is still a problem that needs to be solved [22]. Nanocellulose-based aerogels can be used as an excellent solid support, which can make the recovery process of catalysts easier. However, the wet strength and stability of nanocellulose-based aerogels

are weak in water due to their hydrophilic nature, which extremely limits their applications in wet conditions.

To tackle those as-described problems, here we developed a facile and green way to prepare a robust CNF-based composite aerogel cross-linked with PEI, as well as decorated with Ag NPs. The composite aerogel exhibited the following advantages: I) Eco-friendly bio-based materials. II) Excellent stability and shape-retaining in water conditions. III) Excellent and stable catalytic performance. The Ag NPs were immobilized on the surface of the aerogel walls, which prevents the aggregation of Ag NPs in catalytic reduction process. Moreover, the aerogel membrane also showed stable catalytic activity and fast water transport. IV) Easy to recover and to be reused. The prepared CNF-based composite aerogel served as a monolithic, which is convenient to be used in practical applications. Therefore, this work provides a novel strategy to fabricate a sustainable cellulose-based monolithic, which shows great potential applications in the discoloration of organic dyes in waste streams.

2. Experimental

2.1 Materials

Bleached birch kraft pulp was obtained from a Finnish pulp mill. 2,2,6,6-tetramethylpiperidine-1-oxyl (TEMPO), sodium bromide, sodium hypochlorite solution, silver nitrate ($AgNO_3$), PEI (MW: 70,000, 50% solution in water), sodium borohydride ($NaBH_4$), 4-nitro-phenol (4-NP), methylene blue (MB), and Congo red (CR) were purchased from Sigma Aldrich. All these chemicals used in this work were analytical grade and used without further purification. All aqueous solutions were prepared with deionized water purified by a Milli-Q plus water purification system (Millipore Corporate).

2.2 Methods

2.2.1 Preparation of cellulose nanofibers

The CNFs were exfoliated from bleached birch Kraft pulp according to a previously reported method [36]. In brief, 10 grams of the fiber was disintegrated in 50 mL deionized water before the reaction. The TEMPO (0.125 g) and sodium bromide (1.25 g) were dissolved in 200 mL deionized water and mixed with the fiber suspension, followed by adjusting the pH of the slurry to 10.0 by the addition of 0.5 M NaOH. The oxidation was started by adding the NaClO (5 mmol/g fiber) solution slowly. The pH of the reaction system was maintained at 10 with 0.5 M NaOH for 2 h. The reaction was quenched by ethanol when the pH did not change. Then the fiber was thoroughly washed with water for three times by centrifugation and then sonicated for 5 min at 300 W to obtain CNF aqueous solution with the concentration at 0.6 wt%.

2.2.2 Preparation of CNF/PEI/Ag NPs composite aerogels

25% PEI solution (pH = 10) was added into 5 mL CNF aqueous solution (0.6 wt%, pH = 10) with the weight ratio of 1:1, and stirred for 1 min. The mixed solution was poured into a cylindrical high-density polyethylene (HDPE) cup (40 mm in diameter, 50 mm in height) and stored overnight at room condition. Then the composite aerogel of CNF/PEI was obtained by freeze-drying for 48 h at -52 °C after the sample was frozen at -20 °C for 24 h. The obtained aerogel was immersed into 20 mL $AgNO_3$ solutions with various concentrations at 0.1, 1, and 10 mM for 12 h, and then the aerogel with Ag^+ adsorbed was squeezed and immersed into 20 mL $NaBH_4$ (308 mg, 8.24 mmol) and stirred for 3 h. The obtained composite aerogel was washed thoroughly by deionized water to remove the loosely bound Ag NPs and used for further water treatment. The prepared composite aerogels in these three different $AgNO_3$ solutions were coded as CNF/PEI/Ag NPs-I, CNF/PEI/Ag NPs-II, and CNF/PEI/Ag NPs-III.

2.3 Characterization

2.3.1 X-ray diffraction (XRD)

XRD patterns were collected with a Bruker D8 Discovery (Bruker-AXS, Karlsruhe, Germany) using CuKα radiation ($\lambda = 1.54184$ nm) with a 0.5-mm collimator, a Göbel mirror and a 2D HI-STAR©

detector. The XRD spectra were scanned in the range of 2θ = 7.6°~42.7° by using a 2D Hi-Star detector measuring frames with 600 s/frame at 40 kV and 40 mA.

2.3.2 Thermogravimetric analysis (TGA)

The thermal stability of CNF/PEI, CNF/PEI/Ag NPs-I, CNF/PEI/Ag NPs-II and CNF/PEI/Ag NPs-III were investigated by a Thermal Gravimetric Analyser (Q500, TA instruments). The samples were pre-dried under 40 °C vacuum desiccator before adding into the sample pan for thermal analysis. All the samples were heated at a rate of 10 °C/min from 30 to 900 °C under Nitrogen atmosphere. Sample size was in the range of 2.5-10 mg.

2.3.3 Attenuated total reflectance-infrared spectroscopy (ATR-FTIR)

The FTIR spectra of the composites aerogels were analyzed by a Thermo Scientific Nicolet iS™ 50 FTIR Spectrometer (USA). The spectra were collected with ATR in the absorbance mode from an accumulation of 64 scans in the range of 4000~400 cm^{-1} at a 4 cm^{-1} resolution.

2.3.4 Scanning electron microscopy (SEM)

The cross-sections of the aerogels were imaged by a scanning electron microscope (SEM LEO Gemini 1530 with a ThermoNORAN Vantage X-ray analyzing system manufactured by Thermo Scientific, Germany). The samples were fixed on a sample stage with conductive double-side sticking tape to obtain imagines with an accelerating voltage of 2.7 kV. Elemental analysis of the aerogels of CNF/PEI/Ag NPs was also characterized by an energy dispersive X-ray spectroscopy (EDS) attached to the SEM.

2.3.4 Porosity of the aerogel

Porosity (ρ) was calculated according to the equation:

$$\rho = V_{pore} / V_{sc} * 100 = V_{pore} / (V_{CNF} + V_{pore}) * 100 \quad (1)$$

Where V_{pore} is the volume of pores, V_{sc} is the total volume of the aerogel.

V_{pore} was calculated from the weight difference between dry (m_{dry}) and wet (m_{wet}) sample according to the following equation,

$$V_{pore} = (m_{wet} - m_{dry}) / \rho_{octane} \quad (2)$$

where the density of octane is 0.79 g/cm^3. The CNF volume (V_{CNF}) was calculated by $V_{CNF} = m_{CNF} / \rho_{CNF}$, where density of CNF ($\rho_{CNF}$) was taken as 1.5 g/cm^3.

2.3.5 Catalytic performance tests

The catalytic performance of the CNF/PEI/Ag NPs composite aerogels was evaluated by employing the reduction of 4-NP with $NaBH_4$ as the model reaction. In a typical experiment, the CNF/PEI/Ag NPs composite aerogel was immersed in a solution of $NaBH_4$ (45 mL, 40 mM) and 4-NP (5 mL, 1.2 mM) and stirred slightly to accelerate the mass transfer process. The catalytic process of 4-NP was monitored and recorded by UV-Vis spectroscopy (Shimadzu Co., Japan) at intervals of 1 min.

The discoloration process of dyes was evaluated by immersing the CNF/PEI/Ag NPs composite aerogel into a mixture solution of $NaBH_4$ (10 mL, 50 mM) and dyes (40 mL, 10 mg/L). Here, MB was chosen as a model cationic dye and CR was chosen as a model anionic dye, respectively. The catalytic performance of the composite aerogels on the discoloration of organic dyes was recorded by monitoring the maximum absorbance (λ_{max}) of the dyes with a UV–Vis absorption spectroscopy.

For continuous flow catalytic performance of organic dyes, the composite aerogel of CNF/PEI/Ag NPs (diameter: 24mm; height: 18mm) was packed in a gravity-fed column as a membrane and a solution mixed with NaBH4 (10 mL, 50 mM) and dyes (40 mL, 10 mg/L) flow through the membrane. The mixture solutions before and after passing through the membrane were analyzed by a UV-Vis spectrophotometer. The catalytic discoloration process of MB passing through the membrane was repeated for 10 cycles. Every time before MB passing through the membrane, the membrane was washed with deionized water. The catalytic efficiency of MB was calculated according to the equation:

$$\text{Efficiency (\%)} = 100 *(C_0\text{-}C)/C_0, \quad (3)$$

Where C_0 and C are the concentrations of MB before and after passing through the membrane, respectively.

The permeation flux of the membrane was also calculated according to the following equation:

$$J = V / (A.t) \quad (4)$$

in which V is the volume of the filtrate solution (unit: L), A is the effective membrane filtration area (unit: m^2), and t is the filtration time (unit: h).

3 Results and discussion

The fabrication of the composited aerogel of CNF/PEI/Ag NPs is illustrated in Fig. 1. Firstly, CNFs were produced from bleached birch Kraft pulp by TEMPO oxidation. The carboxylate (-COOH) content of the cellulose nanofibers was 1.2 mmol/g according to the conductivity titration (Fig. S1), which is consistent with the previous work [37]. Then the negatively charged CNFs were cross-linked with a positively charged polymer PEI (MW: 70 000 g/mol) through electrostatic interaction. The CNF/PEI composite aerogel was obtained by freeze-drying. The Ag NPs were then immobilized onto the aerogel surface by immersing the aerogel into $AgNO_3$ solutions at different concentrations and then reduced by $NaHB_4$. In this process, the abundant amine groups ($-NH_2$) on the aerogel fiber surface serve as anchoring sites for Ag^+. Once the Ag^+ was reduced as Ag NPs, they would be captured by the long, branched, and flexible PEI chains. Thereafter, CNF/PEI/Ag NPs composite was formed with a three-dimensionally interconnected and porous structure, which is vital for dye catalytic process.

The morphology and elemental analysis of CNF/PEI/Ag NPs-I, CNF/PEI/Ag NPs-II, and CNF/PEI/Ag NPs-III were characterized by SEM and EDS, respectively (Fig. 2 and Table S1). As seen, heterogeneously shaped micro-sized pores were observed in the cross-section images of all the aerogels. At high magnification, small Ag NPs particles with different size from tens of nanometers to less than 100 nm were observed on the aerogel pore walls. With increasing the concentration of $AgNO_3$ used for the immersion, more Ag NPs was obtained inside the aerogel (Fig. 2 d-e). The porosity of the CNF/PEI/Ag NPs-III was high, up to 96.5 ± 0.8%, as measured using a gravimetric method [38]. The porosity of the aerogel remains high even after introducing a large amount of Ag NPs.

EDS spectra were acquired from several regions on the walls of different CNF/PEI/Ag NPs-III aerogels. The N emission shown in the EDS spectra (13.95 wt%) proved that CNF was successfully cross-linked with PEI and remained after the following washing process. The contents of the elements Cl and Na were 0.37% and 0.19%, respectively, which were close to the detection limit of EDS. For Ag, the content was high, being 22.41 wt%, which confirmed the existence of Ag NPs, but not AgCl in the composite aerogel. The small amount of Cl and Na may come from the preparation process and could not be washed and removed completely. The Properties of CNF/PEI, CNF/PEI/Ag NPs-I, CNF/PEI/Ag NPs-II, and CNF/PEI/Ag NPs-III were shown in Table 1. N_2 adsorption-desorption isotherm curves of these samples (Table S4-7) showed no-porous materials isotherm pattern for their surface area at around 3 m^2g^{-1}. The textural properties of CNF/PEI did not change obviously after introducing Ag NPs, which indicated most of the Ag NPs were evenly dispersed on the surface of the micropore walls.

The crystalline structures of CNF, CNF/PEI, and CNF/PEI/Ag NPs-III were further investigated by X-ray diffraction, as shown in Fig. 3a. The diffraction peaks at $2\theta = 22.5°$ correspond to the (200) lattice planes of cellulose I, which indicates that PEI and Ag NPs did not have an influence on the crystalline structure of CNFs. The pattern of CNF/PEI/Ag NPs-III composite aerogel exhibited five diffraction peaks at $2\theta = 38.0°$, 44.1°, 64.4°, 77.4°, and 81.5°, corresponding to the diffraction of the (111), (200), (220), (311), and (222) [39, 40]. This indicates that the Ag nanocrystals decorated on the aerogel wall were face-centered cubic (fcc) structure, and also confirms that Ag^+ ions were successfully reduced to Ag NPs.

The amount of Ag NPs immobilized inside the aerogel could be tuned by immersing the CNF/PEI aerogel into different $AgNO_3$ concentration solutions (0.1, 1, and 10 mM). As is in Fig. 3b, the amount of Ag NPs inside the aerogel was quantitatively analyzed by TGA. More Ag NPs were reduced on the surface of the pore walls inside the aerogel with increased $AgNO_3$ concentrations. According to the equation: $\phi_{Ag} + 0.105(1- \phi_{Ag}) = x$, in which x is the weight percentage at 500 °C. 0.105 is the

weight percentage of CNF/PEI at 500 °C. The content of Ag NPs reduced inside the aerogel could be regulated from 1.17% to 30.7%.

Fig. 4 shows the FTIR spectra of pure CNF, CNF/PEI, and CNF/PEI/Ag-III aerogels. For the pure CNF aerogel, the characteristic peaks at 3334 cm^{-1} and 1601^{-1} are attributed to –OH stretching vibration and carbonyl groups stretching vibration [41-43]. For the CNF/PEI composite aerogel, the bands at 2842 cm^{-1}, 1556 cm^{-1}, and 1166 cm^{-1} are related to -CH_2- stretching vibrations, -NH_2 and C-C skeleton vibration, respectively [44]. At 3334 cm^{-1}, when the CNF is combined with PEI and Ag NPs, the intensity of –OH groups of CNF/PEI and CNF/PEI/Ag NPs-III aerogels became weaker than that of pure CNF aerogel. In addition, the intensities for the carbonyl groups (1601 cm^{-1}) decreased. These results all suggest that when CNF is combined with PEI and Ag NPs, strong hydrogen bonding and electrostatic interactions in between the hydroxyl, amine, carbonyl groups, and silver NPs feasibly provide a stable 3D network. Meanwhile, the disappearance of the amine band at 1556 cm^{-1} for CNF/PEI/Ag also indicates the hydrogen bonding interactions between amine groups and Ag NPs. Consequently, these strong interactions among the CNF, PEI, and Ag NPs endow the composite aerogel with robust mechanical properties in wet conditions.

In CNF aerogel, the presence of a large amount of carboxyl groups and hydroxyl groups on the surface of the nanofibers formed hydrogen bond networks, which mainly contribute to the strength of CNF aerogel. Once the CNF aerogel was wetted by water, it got broken easily after compression, as seen in Figure 5a. When the CNF aerogel was wetted, the original hydrogen bond network between the nanofibers could be partially broken and replaced by the dissociative H^+ or OH^- in water and then reformed new hydrogen bonds between the dissociative H^+ or OH^- and hydroxyl groups or carboxyl groups on the surface of the cellulose nanofibers [45], the CNF/PEI aerogel showed excellent stability and shape-retaining in water, as shown in Fig. 5b. When the compressive force was released, the aerogel recovered to its original shape immediately by adsorbing water. The wet stability of the CNF/PEI aerogel can be attributed to both large amounts of ionic bonds formed by electrostatic

interaction between the protonated amine groups and carboxyl groups and hydrogen bond networks between amine groups and hydroxyl groups formed [46]. These bonds guaranteed the structural integrity of the 3D network of the aerogel when compressed by external force in water. Due to the synergistic effect of ionic bonds and hydrogen bonds between the CNF and PEI, the composite aerogel showed excellent stability and shape memory in water. Fig. 5c indicates that the immobilization of Ag NPs in the CNF/PEI aerogel did not impair the stability and shape memory property of the aerogel in water, which is vital for the composite aerogel of CNF/PEI/Ag NPs to be used in aqueous conditions for water treatment applications.

Catalytic performance of CNF/PEI/Ag composite

The catalytic activity of the CNF/PEI/Ag aerogels with different loading amount of Ag NPs was evaluated in the reduction reaction of 4-nitrophenol (4-NP) to 4-aminophenol (4-AP) by $NaBH_4$ [22, 47, 48]. The catalytic process was tracked and recorded by UV–vis spectroscopy at room conditions in the characteristic wavelength region centered at 400 nm [49]. As shown in Fig. 6a, b, and c, the intensity of the adsorption peak at 400 nm decreased gradually with time for all samples. As can be seen, the catalytic reduction process goes faster with increasing the amount of Ag NPs, and when the content of Ag NPs was up to 22.4 %, 4-NP could be reduced to 4-AP nearly within 11 mins. During this process, there emerged a new band at around 300 nm, which is the characteristic absorption of 4-AP [50]. Meanwhile, the color of the solution changed from initially yellowish solution to almost colorless water, as displayed as inserted photo in Fig. 6c. These results indicate that the reduction of 4-NP to 4-AP is nearly complete [51]. The catalytic kinetics of the composite aerogels of CNF/PEI/Ag NPs with three different Ag-NPs loading were also investigated. The Ln (A_t/A_0) against reaction time is plotted in Fig. 6d. The liner correlation between Ln (A_t/A_0) versus reaction time (R^2=0.994) confirmed that the reduction of 4-NP catalyzed by all three samples follows a pseudo-zero-order reaction kinetics. Pseudo-zero-order reaction phenomenon is usually observed when the reaction is a heterogeneous catalysis. Here, the Ag NPs immobilized on the surface of the CNF/PEI

aerogel catalyzed the reduction reaction at the aerogel-solution interface (solid-liquid interface). As seen in Fig. 6c, the kinetics constant of the reduction of 4-NP increased when increasing the loading amount of Ag NPs and it can reach 3.6×10^{-3} s^{-1}, which is higher than those previously reported under similar conditions [22, 52-56] (Table 2). The distinguished performance was mainly because of the porous matrix, which ensured the mass transfer and also prevented the Ag NPs from aggregation during the catalyzing process.

In order to evaluate the catalytic discoloration efficiency of the CNF/PEI/Ag NPs-III composite aerogel, MB and CR were chosen as model cationic and anionic dyes in the model reactions, respectively. $NaBH_4$ was selected as a reducing agent. The catalytic discoloration reaction was tracked by UV–vis spectroscopy at room conditions in the characteristic wavelength regions for MB (λmax: 664 nm) and CR (λmax: 498 nm) [21, 57]. Fig. 7a illustrates the discoloration process of an MB solution in the presence of $NaBH_4$ and the CNF/PEI/Ag NPs-III composite aerogel. The maximum absorption peak decreased over time and vanished within 4 min. The discoloration efficiency reached 96% after 4 min. For comparison, the discoloration process of an anionic CR solution was also examined (Fig. 7b). The maximum absorption peak of CR at 498 nm decreased gradually as the catalytic reaction went on and vanished at 21 min. The catalytic reaction time for CR solution (21 min) is obviously much longer than that of MB solution (5 min) at the same conditions. This is mainly because of the chemical structure difference between these two dye molecules. As shown in Figure S 2a, b, the CR molecule ($C_{32}H_{22}N_6Na_2O_6S_2$, MW: 696.7 g/mol) contains two chromogenic bonds (-N=N-) per molecule; however, there is only one chromogenic bond in one MB molecule ($C_{16}H_{18}ClN_3S$, MW: 320 g/mol). Therefore, it takes a longer time for CR solution compared to MB solution in the catalytic discoloration process at the same conditions.

The continuous catalytic discoloration efficiency of the CNF/PEI/Ag NPs-III composite aerogel was also demonstrated by flowing MB or CR and $NaBH_4$ aqueous solution through the 3D CNF/PEI/Ag NPs-III aerogel membrane. The discoloration efficiency of MB before and after passing through the

aerogel was monitored by UV-Vis spectroscopy (Fig. 7c). When the MB solution passed through the aerogel, the characteristic absorbance band at 664 nm completely disappeared. Even for CR, the characteristic absorbance at 498 nm also vanished after passing through the CNF/PEI/Ag NPs-III composite aerogel membrane. The catalytic efficiency of CNF/PEI/Ag NPs-III membrane for the discoloration of MB and CR was 99.2% and 96.4%, which is much higher than previous report on silver-based membrane for catalytic discoloration of MB and CR [57].

The CNF/PEI/Ag NPs-III composite aerogel membrane exhibited excellent water treatment efficiency, evaluated by fluxing the dye solutions through the 3D aerogel membrane. The water flux approached 5×10^4 L m^{-2} h^{-1}, while the initial blue-colored or red-colored solutions became colorless after passing through the aerogel membrane (Fig. 7c, d; Movie S1). Moreover, the CNF/PEI/Ag NPs-III composite aerogel membrane showed excellent MB discoloration performance over a wide range of MB concentrations (Fig. 7e). It is notable that the discoloration efficiency decreased slightly as the MB concentration increases from 5 mg/L to 50 mg/L. Even when the MB concentration was 50 mg/L, the discoloration efficiency was still as high as 94.6%. Fig. 7f shows the catalytic efficiency of MB during the cyclic test of the continuous discoloration process. The catalytic efficiency of MB was still above 98% even after repeating the catalytic process over 10 times. These results indicate that the CNF/PEI/Ag NPs-III composite aerogel membranes possess good catalytic efficiency and recyclability, which are essential for the membranes to be used in industrial applications.

Fig. S3 shows the proposed mechanism of continuous catalytic discoloration reaction. From the SEM results, it is evident that there are large amounts of micropores inside the aerogel, and the Ag NPs are immobilized on the surface wall of the pores. These pores endow the aerogel membrane with a long and distinctive pathway for the solution to pass through. Therefore, when the MB molecules pass through the aerogel, they can have an efficient contact with Ag NPs immobilized on the pore walls. At the same time, the catalytic reaction started in the presence of BH_4^-. In this reaction, Ag NPs are served as an electron relay carrier and initiate the reaction by reacting with BH_4^- to produce negative

charges on the surface of Ag NPs [36, 58]. As shown in Fig. S3, once the MB molecules are in contact with the Ag NPs with negatively charged layer, the chromogenic double bond could be reduced to single bond by accepting electrons from Ag NPs.

4 Conclusion

A facile and green approach was developed to prepare robust 3D CNF-based composite aerogel, in which the CNF was used as a sustainable supporting matrix, the PEI functioned as a crosslinking polymer, and more importantly, the decorated Ag NPs functioned as a catalyst to the discoloration of organic dyes. The as-prepared CNF/PEI/Ag NPs composite aerogel membrane exhibited excellent mechanical stability and shape-retaining property in wet conditions. The catalytic discoloration efficiency was high and stable even when the water flux is high as 5×10^4 L m^{-2} h^{-1}. Additionally, this membrane possesses excellent recyclability and stability after 10 times of cyclic tests of the continuous catalytic discoloration process. This 3D nanocellulose-based aerogel membrane exhibits great potential for treating industrial-scale waste streams.

Acknolwedgement: Zhang W. would like to acknowledge financial support from the China Scholarship Council. This work is also part of the activities within the Johan Gadolin Process Chemistry Centre at Åbo Akademi University.

Reference

[1] H. Hu, J. Xin, H. Hu, X. Wang, D. Miao, Y. Liu, (2015). Synthesis and stabilization of metal nanocatalysts for reduction reactions–a review. Journal of materials chemistry A, 3(21), 11157-11182.

[2] Z. Ren, A. Umble, (2016). Water treatment: Recover wastewater resources locally. Nature, 529(7584), 25.

[3] X. Li, W. Xu,, M. Tang, L. Zhou, B. Zhu, S. Zhu, J. Zhu, (2016). Graphene oxide-based efficient and scalable solar desalination under one sun with a confined 2D water path. Proceedings of the National Academy of Sciences, 113(49), 13953-13958.

[4] C. Liu, D. Kong, P. Hsu, H. Yuan, H. Lee, Y. Liu, P. Maraccini, (2016). Rapid water disinfection using vertically aligned MoS2 nanofilms and visible light. Nature nanotechnology, 11(12), 1098.

[5] K. Yu, S. Yang, C. Liu, H. Chen, H. Li, C. Sun, S. Boyd, (2012). Degradation of organic dyes via bismuth silver oxide initiated direct oxidation coupled with sodium bismuthate based visible light photocatalysis. Environmental science & technology, 46(13), 7318-7326.

[6] V. Sakkas, M. Islam, C. Stalikas, T. Albanis, (2010). Photocatalytic degradation using design of experiments: a review and example of the Congo red degradation. Journal of hazardous materials, 175(1-3), 33-44.

[7] J. Tiwari, K. Mahesh, N. Le, K. Kemp, R. Timilsina, R. Tiwari, K. Kim, (2013). Reduced graphene oxide-based hydrogels for the efficient capture of dye pollutants from aqueous solutions. Carbon, 56, 173-182.

[8] T. Zhu, J. Chen, X. Lou, (2012). Highly efficient removal of organic dyes from waste water using hierarchical NiO spheres with high surface area. The Journal of Physical Chemistry C, 116(12), 6873-6878.

[9] B. Ramalingam, M. Khan, B. Mondal, A. Mandal, S. Das, (2015). Facile synthesis of silver nanoparticles decorated magnetic-chitosan microsphere for efficient removal of dyes and microbial contaminants. ACS Sustainable Chemistry & Engineering, 3(9), 2291-2302.

[10] F. Han, V. Kambala, M. Srinivasan, D. Rajarathnam, R. Naidu, (2009). Tailored titanium dioxide photocatalysts for the degradation of organic dyes in wastewater treatment: a review. Applied Catalysis A: General, 359(1-2), 25-40.

[11] C. Martínez-Huitle, E. Brillas, (2009). Decontamination of wastewaters containing synthetic organic dyes by electrochemical methods: a general review. Applied Catalysis B: Environmental, 87(3-4), 105-145.

[12] F. Jiang, D. Dinh, Y. Hsieh, (2017). Adsorption and desorption of cationic malachite green dye on cellulose nanofibril aerogels. Carbohydrate polymers, 173, 286-294.

[13] J. Abdi, M. Vossoughi, N. Mahmoodi, I. Alemzadeh, (2017). Synthesis of metal-organic framework hybrid nanocomposites based on GO and CNT with high adsorption capacity for dye removal. Chemical Engineering Journal, 326, 1145-1158.

[14] L. Lv, X. Han, L. Zong, M. Li, J. You, X. Wu, C. Li, (2017). Biomimetic hybridization of Kevlar into silk fibroin: Nanofibrous strategy for improved mechanic properties of flexible composites and filtration membranes. ACS nano, 11(8), 8178-8184.

[15] K. Thebo, X. Qian, Q. Zhang, L. Chen, H. Cheng, W. Ren, (2018). Highly stable graphene-oxide-based membranes with superior permeability. Nature communications, 9(1), 1486.

[16] P. He, X. Tang, L. Chen, P. Xie, L. He, H. Zhou, T. Fan, (2018). Patterned Carbon Nitride–Based Hybrid Aerogel Membranes via 3D Printing for Broadband Solar Wastewater Remediation. Advanced Functional Materials, 28(29), 1801121.

[17] Y. Zhang, Z. Zhou, Y. Shen, Q. Zhou, J. Wang, A. Liu, Y. Zhang, (2016). Reversible assembly of graphitic carbon nitride 3D network for highly selective dyes absorption and regeneration. ACS nano, 10(9), 9036-9043.

[18] X. Qian, Y. Wu, M. Kan, M. Fang, D. Yue, J. Zeng, Y. Zhao, (2018). FeOOH quantum dots coupled g-C3N4 for visible light driving photo-Fenton degradation of organic pollutants. Applied Catalysis B: Environmental, 237, 513-520.

[19] L. Zhou, J. Lei, L. Wang, Y. Liu, J. Zhang, (2018). Highly efficient photo-Fenton degradation of methyl orange facilitated by slow light effect and hierarchical porous structure of Fe2O3-SiO2 photonic crystals. Applied Catalysis B: Environmental, 237, 1160-1167.

[20] Y. Wang, L. Zhu, J. You, F. Chen, L. Zong, X. Yan, C. Li, (2017). Catecholic coating and silver hybridization of chitin nanocrystals for ultrafiltration membrane with continuous flow catalysis and gold recovery. ACS Sustainable Chemistry & Engineering, 5(11), 10673-10681.

[21] J. Gu, C. Hu, W. Zhang, A. Dichiara, (2018). Reagentless preparation of shape memory cellulose nanofibril aerogels decorated with Pd nanoparticles and their application in dye discoloration. Applied Catalysis B: Environmental, 237, 482-490.

[22] X. An, Y. Long, Y. Ni, (2017). Cellulose nanocrystal/hexadecyltrimethylammonium bromide/silver nanoparticle composite as a catalyst for reduction of 4-nitrophenol. Carbohydrate polymers, 156, 253-258.

[23] W. Sun, C. Zhang, J. Chen, B. Zhang, H. Zhang, Y. Zhang, L. Chen, (2017). Accelerating biodegradation of a monoazo dye Acid Orange 7 by using its endogenous electron donors. Journal of hazardous materials, 324, 739-743.

[24] S. Sun, S. Xie, H. Chen, Y. Cheng, Y. Shi, X. Qin, J. Yuan, (2016). Genomic and molecular mechanisms for efficient biodegradation of aromatic dye. Journal of hazardous materials, 302, 286-295.

[25] M. Oveisi, M. Asli, N. Mahmoodi, (2018). MIL-Ti metal-organic frameworks (MOFs) nanomaterials as superior adsorbents: Synthesis and ultrasound-aided dye adsorption from multicomponent wastewater systems. Journal of hazardous materials, 347, 123-140.

[26] O. Yehezkeli, D. de Oliveira, J. Cha, (2015). Electrostatically Assembled CdS–Co3O4 Nanostructures for Photo-assisted Water Oxidation and Photocatalytic Reduction of Dye Molecules. Small, 11(6), 668-674.

[27] V. Vaiano, M. Matarangolo, O. Sacco, D. Sannino, (2017). Photocatalytic treatment of aqueous solutions at high dye concentration using praseodymium-doped ZnO catalysts. Applied Catalysis B: Environmental, 209, 621-630.

[28] V. Vaiano, O. Sacco, D. Sannino, P. Ciambelli, (2015). Nanostructured N-doped TiO2 coated on glass spheres for the photocatalytic removal of organic dyes under UV or visible light irradiation. Applied Catalysis B: Environmental, 170, 153-161.

[29] A. Rostami-Vartooni, M. Nasrollahzadeh, M. Alizadeh, (2016). Green synthesis of seashell supported silver nanoparticles using Bunium persicum seeds extract: application of the particles for catalytic reduction of organic dyes. Journal of colloid and interface science, 470, 268-275.

[30] M. Kaushik, A. Moores, (2016). nanocelluloses as versatile supports for metal nanoparticles and their applications in catalysis. Green Chemistry, 18(3), 622-637.

[31] B. Thomas, M. Raj, J. Joy, A. Moores, G. Drisko, C. Sanchez, (2018). Nanocellulose, a versatile green platform: from biosources to materials and their applications. Chemical reviews, 118(24), 11575-11625.

[32] M. Rajinipriya, M. Nagalakshmaiah, M. Robert, S. Elkoun, (2018). Importance of agricultural and industrial waste in the field of nanocellulose and recent industrial developments of wood based nanocellulose: a review. ACS Sustainable Chemistry & Engineering, 6(3), 2807-2828.

[33] H. Khalil, Y. Davoudpour, M. Islam, A. Mustapha, K. Sudesh, R. Dungani, M. Jawaid, (2014). Production and modification of nanofibrillated cellulose using various mechanical processes: a review. Carbohydrate polymers, 99, 649-665.

[34] B. Pang, H. Liu, P. Liu, X. Peng, K. Zhang, (2018). Water-in-oil Pickering emulsions stabilized by stearoylated microcrystalline cellulose. Journal of colloid and interface science, 513, 629-637.

[35] X. An, Y. Long, Y. Ni, (2017). Cellulose nanocrystal/hexadecyltrimethylammonium bromide/silver nanoparticle composite as a catalyst for reduction of 4-nitrophenol. Carbohydrate polymers, 156, 253-258.

[36] Y. Zhang, P. Zhu, L. Chen, G. Li, F. Zhou, D. Lu, C. Wong, (2014). Hierarchical architectures of monodisperse porous Cu microspheres: synthesis, growth mechanism, high-efficiency and recyclable catalytic performance. Journal of Materials Chemistry A, 2(30), 11966-11973.

[37] C. Xu, B. Molino, X. Wang, F. Cheng, W. Xu, P. Molino, G. Wallace, (2018). 3D printing of nanocellulose hydrogel scaffolds with tunable mechanical strength towards wound healing application. Journal of Materials Chemistry B, 6(43), 7066-7075.

[38] C. Pandis, S. Madeira, J. Matos, A. Kyritsis, J. Mano, J. Ribelles, (2014). Chitosan–silica hybrid porous membranes. Materials Science and Engineering: C, 42, 553-561.

[39] Y. Yang, Z. Chen, X. Wu, X. Zhang, G. Yuan, (2018). Nanoporous cellulose membrane doped with silver for continuous catalytic decolorization of organic dyes. Cellulose, 25(4), 2547-2558.

[40] Y. Wang, L. Zhu, J. You, F. Chen, L. Zong, X. Yan, C. Li, (2017). Catecholic coating and silver hybridization of chitin nanocrystals for ultrafiltration membrane with continuous flow catalysis and gold recovery. ACS Sustainable Chemistry & Engineering, 5(11), 10673-10681.

[41] W. Zhang, Z. Jing, Y. Shan, X. Ge, X. Mu, Y. Jiang, P. Wu, (2016). Paper reinforced with regenerated cellulose: a sustainable and fascinating material with good mechanical performance, barrier properties and shape retention in water. Journal of Materials Chemistry A, 4(44), 17483-17490.

[42] A. Salama, N. Shukry, M. El-Sakhawy, (2015). Carboxymethyl cellulose-g-poly (2-(dimethylamino) ethyl methacrylate) hydrogel as adsorbent for dye removal. International journal of biological macromolecules, 73, 72-75.

[43] J. Breton, C. Boullais, G. Berger, C. Mioskowski, E. Nabedryk, (1995). Binding sites of quinones in photosynthetic bacterial reaction centers investigated by light-induced FTIR difference spectroscopy: symmetry of the carbonyl interactions and close equivalence of the QB vibrations in Rhodopseudomonas sphaeroides and Rhodobacter viridis probed by isotope labeling. Biochemistry, 34(36), 11606-11616.

[44] N. Zhang, G. Zang, C. Shi, H. Yu, G. Sheng, (2016). A novel adsorbent TEMPO-mediated oxidized cellulose nanofibrils modified with PEI: Preparation, characterization, and application for Cu (II) removal. Journal of hazardous materials, 316, 11-18.

[45] J. Cai, L. Zhang, C. Chang, G. Cheng, X. Chen, B. Chu, (2007). Hydrogen-bond-induced inclusion complex in aqueous cellulose/LiOH/urea solution at low temperature. ChemPhysChem, 8(10), 1572-1579.

[46] Z. Sui, Y. Cui, J. Zhu, B. Han, (2013). Preparation of three-dimensional graphene oxide–polyethylenimine porous materials as dye and gas adsorbents. ACS applied materials & interfaces, 5(18), 9172-9179.

[47] M. Guo, J. He, Y. Li, S. Ma, X. Sun, (2016). One-step synthesis of hollow porous gold nanoparticles with tunable particle size for the reduction of 4-nitrophenol. Journal of hazardous materials, 310, 89-97.

[48] S. Gao, Z. Zhang, K. Liu, B. Dong, (2016). Direct evidence of plasmonic enhancement on catalytic reduction of 4-nitrophenol over silver nanoparticles supported on flexible fibrous networks. Applied Catalysis B: Environmental, 188, 245-252.

[49] H. Qian, Q. He, J. Zheng, S. Li, S. Zhang, (2014). Catechol-functionalized microporous organic polymer as supported media for Pd nanoparticles and its high catalytic activity. Polymer, 55(2), 550-555.

[50] J. Kim, M. Cha, J. Lee, T. Choi, J. Chang, (2017). Preparation of a sulfur-functionalized microporous polymer sponge and in situ growth of silver nanoparticles: a compressible monolithic catalyst. ACS applied materials & interfaces, 9(43), 38081-38088.

[51] W. Xiao, Y. Zhang, B. Liu, (2015). Raspberrylike SiO2@ reduced graphene oxide@ AgNP composite microspheres with high aqueous dispersity and excellent catalytic activity. ACS applied materials & interfaces, 7(11), 6041-6046.

[52] P. Liu, M. Zhao, (2009). Silver nanoparticle supported on halloysite nanotubes catalyzed reduction of 4-nitrophenol (4-NP). Applied Surface Science, 255(7), 3989-3993.

[53] I. Ahmad, T. Kamal, S. Khan, A. Asiri, (2016). An efficient and easily retrievable dip catalyst based on silver nanoparticles/chitosan-coated cellulose filter paper. Cellulose, 23(6), 3577-3588.

[54] P. Xu, C. Cen, N. Chen, H. Lin, Q. Wang, N. Xu, Z. Teng, (2018). Facile fabrication of silver nanoparticles deposited cellulose microfiber nanocomposites for catalytic application. Journal of colloid and interface science, 526, 194-200.

[55] Lu Y, Spyra P, Mei Y, et al. Composite hydrogels: robust carriers for catalytic nanoparticles[J]. Macromolecular Chemistry and Physics, 2007, 208(3): 254-261.

[56] Tang S, Vongehr S, Meng X. Carbon spheres with controllable silver nanoparticle doping[J]. The Journal of Physical Chemistry C, 2009, 114(2): 977-982.

[57] N. Liu, W. Zhang, X. Li, R. Qu, Q. Zhang, Y. Wei, L. Jiang, (2017). Fabrication of robust mesh with anchored Ag nanoparticles for oil removal and in situ catalytic reduction of aromatic dyes. Journal of Materials Chemistry A, 5(30), 15822-15827.

[58] Z. Jiang, C. Liu, L. Sun, (2005). Catalytic properties of silver nanoparticles supported on silica spheres. The Journal of Physical Chemistry B, 109(5), 1730-1735.

Figures and figure captions

Fig. 1. Schematic illustration on the fabrication of the composite aerogel of CNF/PEI/Ag NPs. From left to right: 1Production cellulose nanofibers; 2 Preparation CNF/PEI composite aerogel; 3 Immobilization of Ag NPs into the CNF/PEI composite aerogel.

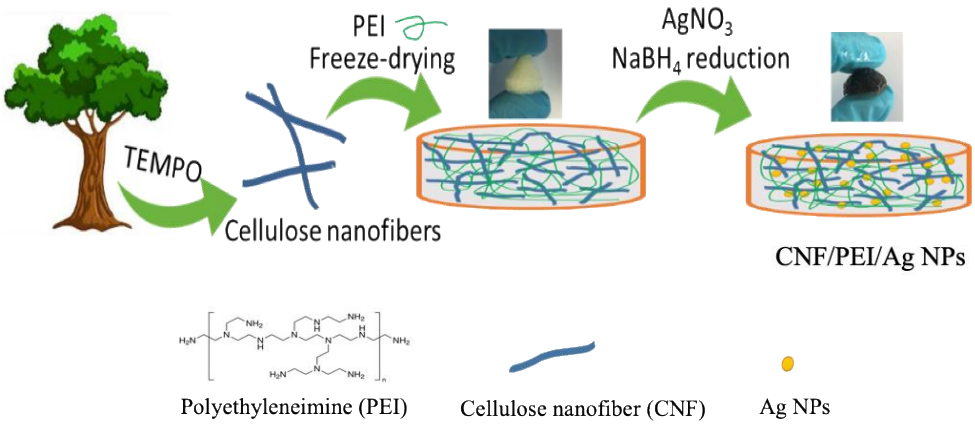

Fig. 2. SEM images of the CNF/PEI/Ag NPs-I (a, d), CNF/PEI/Ag NPs-II (b, e) and CNF/PEI/Ag NPs-III (c, f) aerogels and EDS spectrum of the CNF/PEI/Ag NPs-III aerogel (g). The scale bar: 100 µm (a, b, c) and 200 nm (d, e, f).

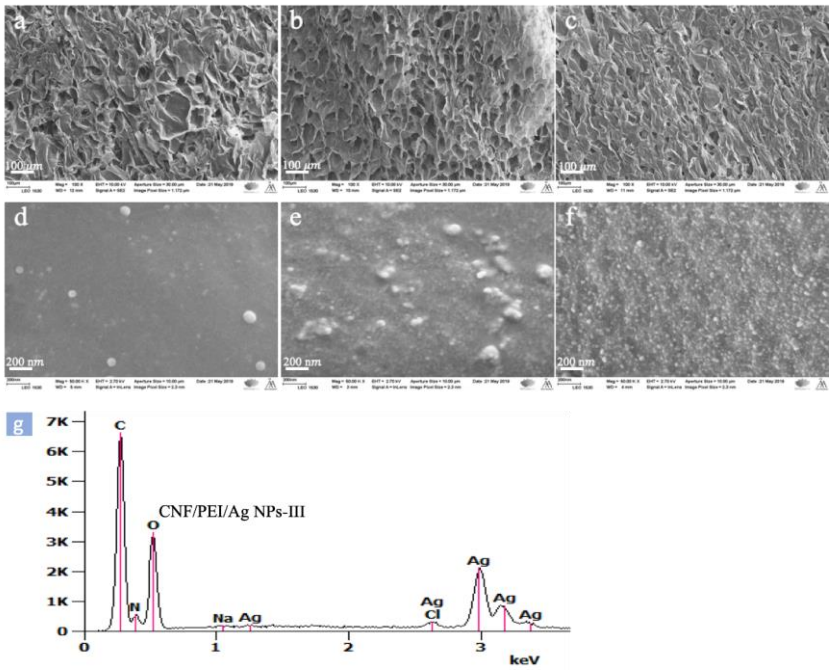

Table 1. Propersties of CNF/PEI, CNF/PEI/Ag NPs-I, CNF/PEI/Ag NPs-II, and CNF/PEI/Ag NPs-III

Sample	BET surface area (m^2g^{-1})	Porosity (%)	Density (mg cm^{-3})	Ag NPs content (%)
CNF/PEI	<3.5	97.6	9.92	0
CNF/PEI/Ag NPs-I	<3.5	97.4	10.48	4.7
CNF/PEI/Ag NPs-II	<3.5	96.2	11.77	15.5
CNF/PEI/Ag NPs-III	<3.5	96.5	14.89	22.4

Fig. 3. (a) XRD patterns of CNF, CNF/PEI, CNF/PEI/Ag NPs-III aerogels; (b) TGA results of CNF/PEI, CNF/PEI/Ag NPs-I, CNF/PEI/Ag NPs-II and CNF/PEI/Ag NPs-III.

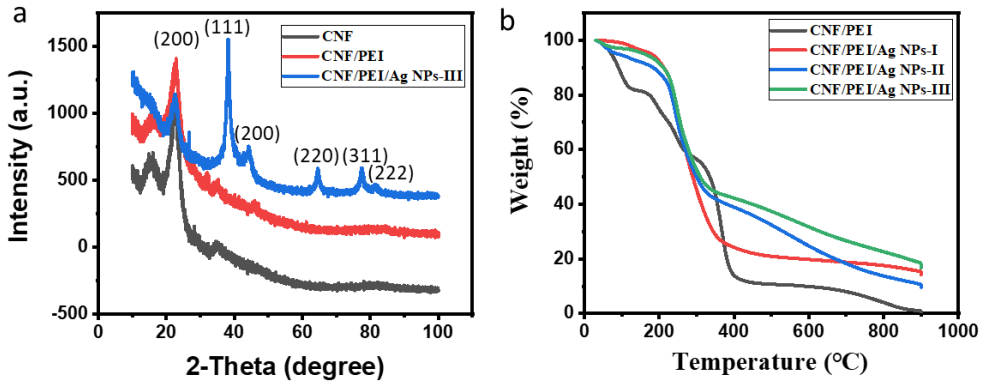

Fig. 4. FTIR of pure CNF (black line), CNF/PEI (red line), and CNF/PEI/Ag-III (blue line).

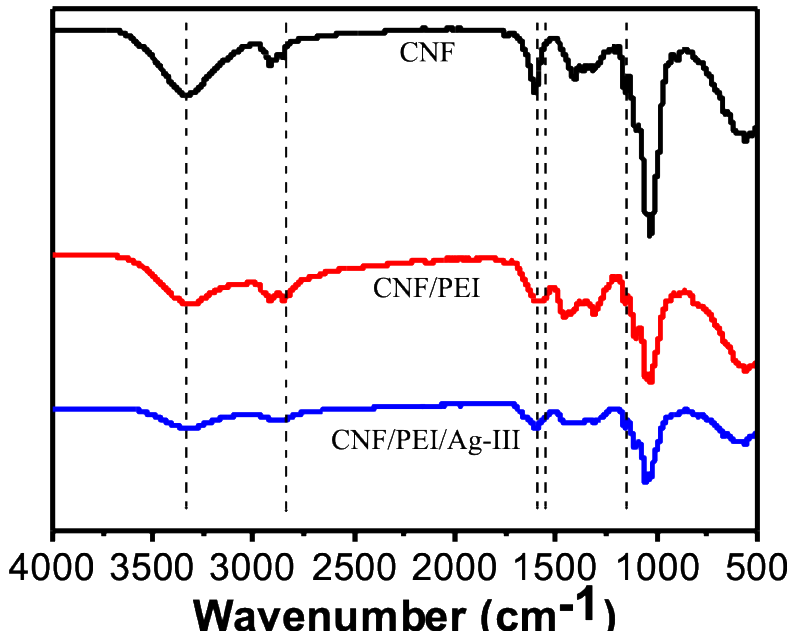

Fig. 5. Wet stability and shape-retaining in water: a) pure CNF aerogel was broken in water after pressing, b) CNF/PEI aerogel can remain its shape in water after pressing, c) CNF/PEI/Ag NPs-III can remain its shape in water after pressing.

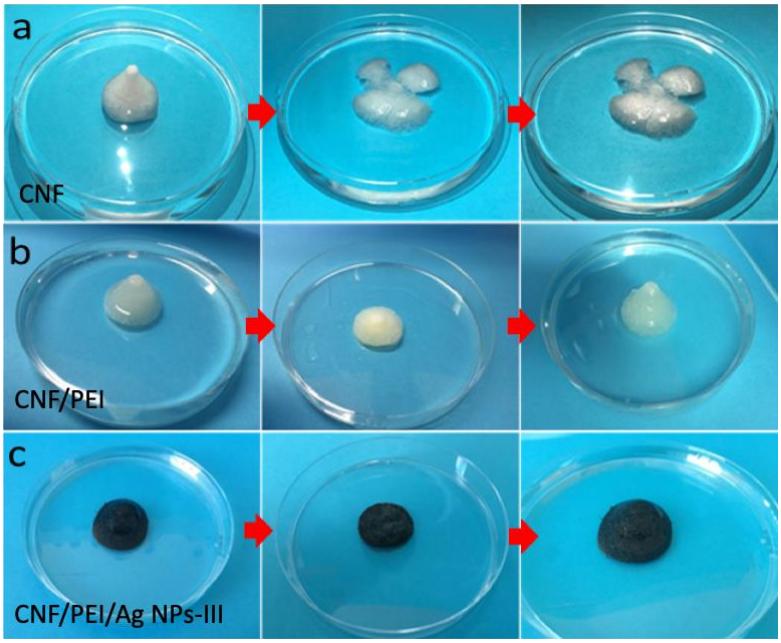

Fig. 6. Time-dependent (min) successive UV-Vis spectra of the reduction of 4-NP a, b and c catalyzed by CNF/PEI/Ag aerogels with different amount of Ag NPs (a: CNF/PEI/Ag NPs-I; b: CNF/PEI/Ag NPs-II; c: CNF/PEI/Ag NPs-III) and digital camera photograph for the reduction of 4-NP; d) Effect of Ag NPs amount on the reduction rate (Ln (A_t/A_0) against time) of different composite aerogels.

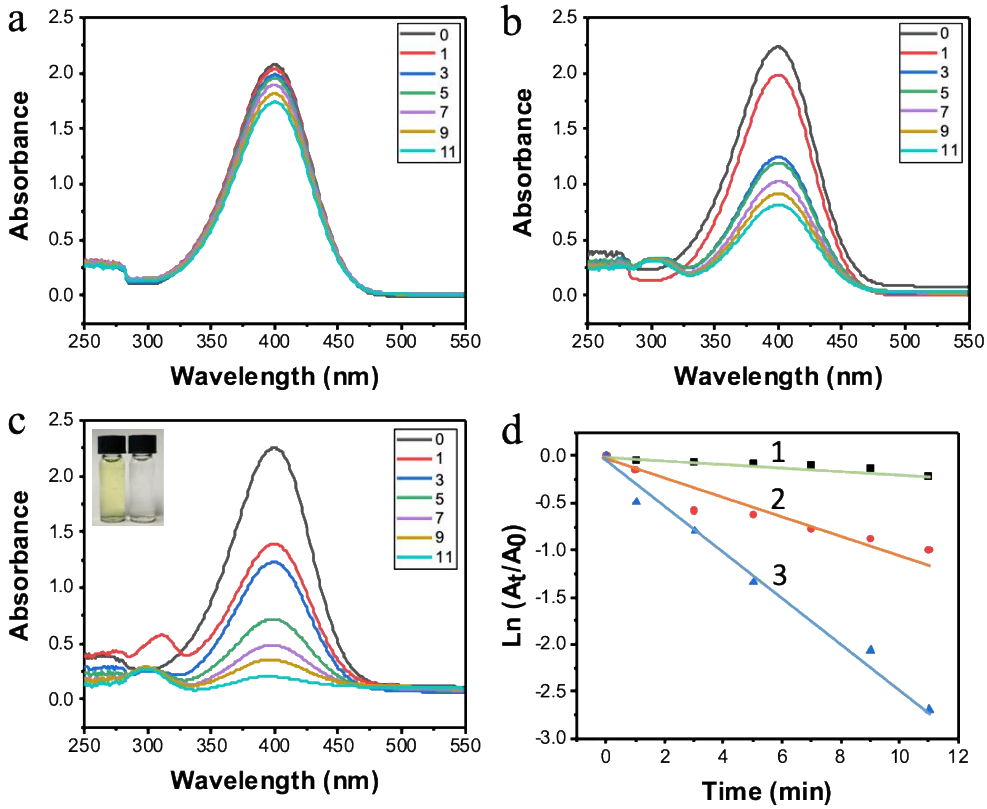

613 Table 2 Comparison of rate constant for 4-nitrophenol reduction by AgNP-based composite catalysts.

Sample	Rate constant(k) x 10^{-3} (s^{-1})	Reference
CNC/ CTAB/ Ag nanohybrid	1.6	22
PVA/PS-PEG MA/Ag	0.078	55
Ag/C spheres	1.69	56
Silver nanoparticle/halloysite nanotubes	0.27	52
silver nanoparticles/chitosan/ cellulose filter paper	1.7	53
Silver Nanoparticles Deposited Cellulose Microfiber	2.4	54
Nanocellulose/silver nanoparticle aerogel	3.6	This work

614

615

616

617

618

619

620

621

622

623

Fig. 7. Successive UV-vis spectra of the reduction of MB(a) and CR(b) catalyzed by CNF/PEI/Ag NPs-III aerogel. UV-Vis spectra for the MB(c) and CR(d) solutions before and after passing through the CNF/PEI/Ag NPs-III aerogel membrane. e) The degradation efficiency at different concentrations of the MB solution. f) The conversion rate of MB during the cyclic test of the continuous catalytic decolorization process.